

## Long-range ordered nanoaperture array with uniform diameter and interpore spacing

Ming-Nung Lin

*Department of Physics, National Taiwan University, Taipei 106, Taiwan*

Minn-Tsong Lin<sup>a)</sup>

*Department of Physics, National Taiwan University, Taipei 106, Taiwan and Institute of Atomic and Molecular Sciences, Academia Sinica, Taipei, Taiwan*

C. Y. Liu and M. Y. Lai

*Institute of Atomic and Molecular Sciences, Academia Sinica, P. O. Box 23-166, Taipei 106, Taiwan*

N. W. Liu

*Institute of Atomic and Molecular Sciences, Academia Sinica, P. O. Box 23-166, Taipei 106, Taiwan and Department of Materials Science and Engineering, National Taiwan University, Taipei 106, Taiwan*

C. Y. Peng, H. H. Wang, and Y. L. Wang<sup>b)</sup>

*Institute of Atomic and Molecular Sciences, Academia Sinica, P. O. Box 23-166, Taipei 106, Taiwan and Department of Physics, National Taiwan University, Taipei 106, Taiwan*

(Received 27 May 2005; accepted 20 September 2005; published online 20 October 2005)

In application of focused-ion-beam lithography and grazing Ar<sup>+</sup> milling on the U-shape barrier layer of anodic alumina nanochannels, we fabricated a hexagonally symmetry aperture array with nominal diameter of  $12 \pm 2$  nm and interspacing of  $100 \pm 2$  nm. Besides long-range spatial ordering, the focused-ion-beam guided-grown process has also significantly improved uniformity of both the interpore spacing and the aperture size. This aperture array membrane can be applied to the fabrication of nanostructures, such as a lithographic contact mask for ordered quantum-dot array.

© 2005 American Institute of Physics. [DOI: [10.1063/1.2117608](https://doi.org/10.1063/1.2117608)]

Recently, self-assembly properties of patterned materials on the nanoscale have attracted more and more interest.<sup>1-3</sup> One of the important nanostructures is the self-organized hexagonally anodic alumina ordered array of nanochannels. With its highly uniform and straight nanopore structure, and its extremely high-density advantages, an anodic alumina oxide (AAO) nanochannel is extensively applied to advanced nanodevices, such as carbon nanotube arrays, for flat panel displays,<sup>4</sup> magnetic storage media,<sup>5</sup> and single electronics.<sup>6</sup> By a two-step anodization, AAO nanochannels self-organize into hexagonally close packed (hcp) domains with an average size of a few micrometers.<sup>7</sup> Even though the nanochannels of such self-organized arrays also exhibit improved size uniformity, the presence of irregular channels along the domain boundaries sets a severe limitation on its further improvement. To overcome this drawback, five approaches have been developed to fabricate an ideally ordered nanochannel array on AAO film: Nanoimprint lithography,<sup>8-10</sup> electron-beam lithography,<sup>11</sup> direct focused-ion-beam (FIB) lithography,<sup>12,13</sup> holographic lithography,<sup>14</sup> and resist-assisted FIB lithography.<sup>15</sup> These lithographic methods first create an ordered array of concaves on the Al surface and then use the concaves as “pinning points” to align the orientation of the nanochannel domains and therefore completely eliminate the presence of domain boundaries. Especially for nanoimprint and holographic lithography, the monodomain area can reach to  $\sim \text{cm}^2$ .<sup>10,14</sup> Besides the long-range ordered structure, many research groups<sup>16-18</sup> are actively seeking the way to fabricate the AAO with a smaller pore size; however, it is rather difficult to ideally

fabricate ordered AAO with a pore size less than 20 nm for the natural limit caused by the lithography.<sup>16-18</sup> On the other hand, the pore diameter of nanochannels is 40% of the interspacing, which severely limits the application possibilities when both a large interspacing and a small pore diameter are required. In this letter, we use grazing Ar<sup>+</sup> milling to shrink down and control the pore or aperture diameter of an ideally ordered nanochannel array. By this way, we fabricated a hcp nanoaperture array with a nominal diameter of  $12 \pm 2$  nm and interspacing of  $100 \pm 2$  nm.

Figure 1 represents the process of the sample preparation. High-purity Al (99.99%) is electropolished in a mixture solution of HClO<sub>4</sub> and C<sub>2</sub>H<sub>5</sub>OH (ratio 1:5) at 5 °C under constant stirring. A commercial 50 keV Ga FIB with a beam diameter  $\sim 10$  nm and a beam current  $\sim 1.1$  pA is utilized to create an array of hcp concaves on a polished Al surface. These concaves are employed to guide the anodization growth process of nanochannels. We use 0.3 M oxalic acid

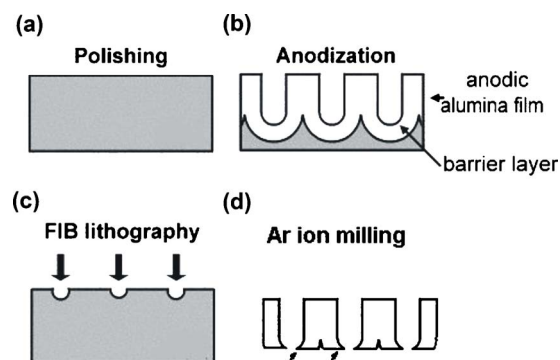


FIG. 1. Schematic diagram showing the process for fabrication of the nano-pattern apertures.

<sup>a)</sup>Electronic mail: [mtlin@phys.ntu.edu.tw](mailto:mtlin@phys.ntu.edu.tw)

<sup>b)</sup>Electronic mail: [ylwang@pub.iam.s.sinica.edu.tw](mailto:ylwang@pub.iam.s.sinica.edu.tw)

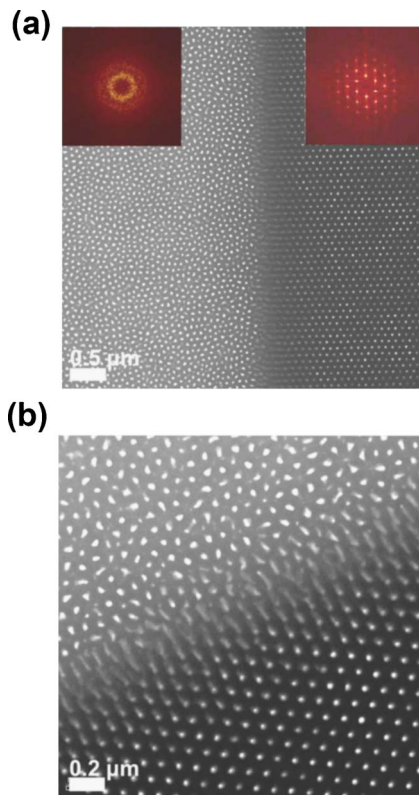


FIG. 2. TEM image with a boundary between the two areas of different growth modes. The insets are the Fourier transform for the FIB-guided area (right corner), and self-organized area (left corner), respectively.

solution to create nanochannels with 100 nm interspacing at 4 °C and 40 V anodization voltage. The remaining Al substrate is removed by a  $\text{CuCl}_2$  solution (3%) in order to expose the naked barrier. An  $\text{Ar}^+$  beam miller machine MPS-3000 PBN is set up to sputter the U-shaped barrier layer in order to create the nanoapertures. The  $\text{Ar}^+$  beam current density is approximately  $1.2 \text{ mA cm}^{-2}$  with a beam energy 500 eV. The incident  $\text{Ar}^+$  beam was tilted by an angle around  $75^\circ$  to control the aperture size. Finally, the images of nanoapertures are taken by transmission electron microscope (TEM). By taking the top view of the thin ( $\sim 150 \text{ nm}$ ) alumina film, the electrons directly passing through the apertures without any interceptions will project these apertures to form the shining spots image on the screen.

Figure 2 represents the TEM image with a boundary between the two areas of both growth modes with (left-hand side) and without (right-hand side) FIB-guided prepatterning. The array comprised by FIB-guided channels has increased not only the degree of order of the nanoapertures but also their inter-pore spacing and aperture size. In contrast, the array comprised of a self-organized channel loses the long-range order and reveals a dispersive distribution in its inter-pore spacing and aperture size. Fourier transform was made for each area in order to further clarify the differences between two areas. In the self-organized area, the emerging peaks of the Fourier transform form an isotropic ring pattern, indicating the absence of a long-range ordering in the FIB-guided area; the hexagonally arranged peaks are sharp. This can be connected to the improvement of the degree of order in the orientation arrangement of the nanochannels.

Figures 3(a) and 3(b) show the TEM images of the nanoapertures in a self-organized area on different scales. It

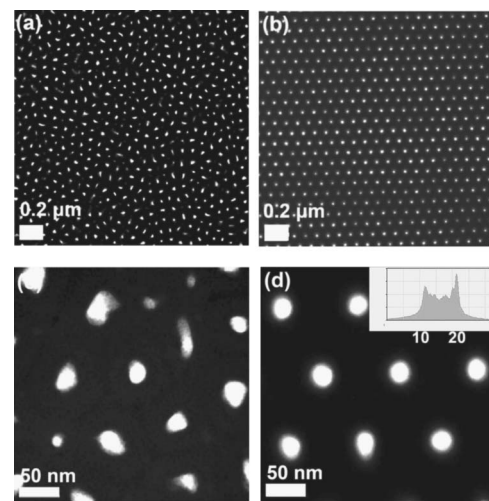


FIG. 3. TEM images of the randomly selected area in different scales, the inset is the profile of the selected aperture (the middle one in the bottom line).

can be obviously seen that the size distribution of these apertures [Fig. 3] is relatively broad. Besides, the shapes of these apertures are irregular and the inter-pore spacing between each neighboring apertures are diverse. Figures 3(c) and 3(d) show the TEM images of the nanoapertures in a FIB-guided area on different scales. These apertures are mostly round shaped, and reveal a uniform size distribution with a diameter of 12 nm. Moreover, the inter-pore spacing between these neighboring apertures is 100 nm.

Two distinct characteristics in these TEM images should be discussed in more details. First, the electrons passing through these apertures were indeed exposed to form the shining spots in the TEM images. The contrast is good enough to clarify the differences between apertures and nearby alumina areas. Second, the shining spot in the TEM image is the projection of the transmitted electron beam through the whole channel; therefore, there are two important factors that affect the certification of the aperture size. Both the roughness of the channel wall and the inclined angle of the pore will modify the projection image of the electron beam. Thus, the nominal diameter of the apertures obtained from the TEM image also reflects the overall effect of geometrical factors mentioned above on electron transmission.

Finally, a statistical analysis in the geometrical distribution was made in order to have a clear comparison between the different nanoapertures from two growth modes. We randomly chose 100 apertures to measure diameter size of aperture. The size distribution of nanoapertures is shown in Fig. 4. The mean value of the FIB-guided aperture size is 12 nm with dispersion  $\pm 2 \text{ nm}$ . More than 80% of the aperture sizes are distributed between 11–13 nm. The mean value of the inter-pore spacing is 100 nm with a dispersion of  $\pm 2 \text{ nm}$ . On the other hand, the average size of the apertures made from the self-organized AAO is 13 nm, however, with a much larger dispersion of  $\pm 6 \text{ nm}$ . Less than 35% of the aperture sizes are spread between 12–14 nm. The mean value of inter-pore spacing is 102 nm with a dispersion  $\pm 25 \text{ nm}$ . These distinct differences can be mainly ascribed to two reasons. First, the aperture size depends on the pore size and curvature of the barrier layer with the same inclined grazing  $\text{Ar}^+$  milling angle. The size distribution and the interspacing

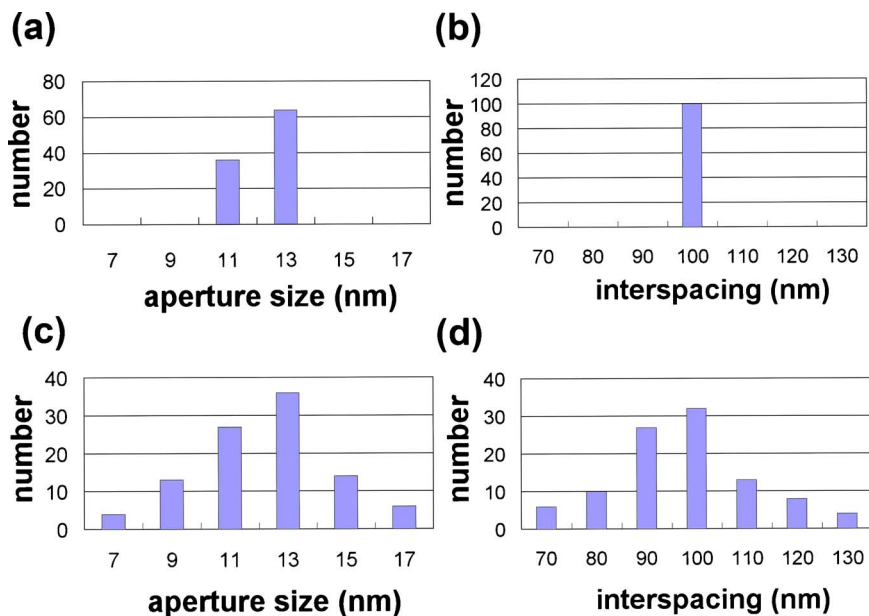


FIG. 4. The statistical analysis for two growth modes: (a) Aperture size distribution in FIB-guided area; (b) interspacing distribution in FIB-guided area; (c) aperture size distribution in self-organized area; and (d) interspacing distribution in self-organized area.

between neighboring channels were demonstrated to be excellently uniform in the FIB-guided sample.<sup>6</sup> In contrast, the self-organized sample cannot achieve such uniformity. Second, the relative height around neighboring channels also affects the aperture size. The lower channel (compared to nearby channels) will be shielded by its neighbors under the inclined grazing Ar<sup>+</sup> beam and then this results in the smaller aperture. Compared to the self-organized mode, the growth rate of the FIB-guided channels is more identical and this leads to same height of each channel.

In conclusion, we demonstrated a combined process of focused-ion-beam-guided prepatterning technique and grazing Ar<sup>+</sup> milling to fabricate long-range ordered nanoaperture arrays. The nominal diameter of the created apertures is  $12 \pm 2$  nm and the interspacing is  $100 \pm 2$  nm. Compared to the self-organized process, the focused-ion-beam-guided process has increased not only long-range order but also uniformity of the aperture size as well as the interpore spacing. This technique could be extensively applied to the manufacturing of advanced nanodevices with requirement of high nanoscale ordering in a large area.<sup>4,5,19,20</sup>

<sup>1</sup>J. L. Wilbur and G. M. Whitesides *Nanotechnology*, edited by G. Timp (Springer, Berlin, 1999), p. 331.

<sup>2</sup>S. Gwo, C.-P. Chou, C.-L. Wu, Y.-J. Ye, S.-J. Tsai, W.-C. Lin,

and M.-T. Lin, *Phys. Rev. Lett.* **90**, 185506 (2003).

<sup>3</sup>W.-C. Lin, C.-C. Kuo, M.-F. Luo, K.-J. Song, and M.-T. Lin, *Appl. Phys. Lett.* **86**, 043105 (2005).

<sup>4</sup>J. S. Suh and J. S. Lee, *Appl. Phys. Lett.* **75**, 2047 (1999).

<sup>5</sup>K. Nielsch, R. B. Wehrspohn, J. Barthel, J. Kirschner, and U. Gösele, *Appl. Phys. Lett.* **79**, 1360 (2001).

<sup>6</sup>N. Kouklin and L. Menon, *Appl. Phys. Lett.* **80**, 1649 (2002).

<sup>7</sup>H. Masuda and K. Fukada, *Science* **268**, 1466 (1995).

<sup>8</sup>H. Masuda, H. Yamada, M. Satoh, and H. Asoh, *Appl. Phys. Lett.* **71**, 2770 (1997).

<sup>9</sup>H. Masuda, A. Abe, M. Nakao, A. Yokoo, T. Tamamura, and K. Nishio, *Adv. Mater. (Weinheim, Ger.)* **15**, 161 (2003).

<sup>10</sup>J. Choi, K. Nielsch, M. Reiche, R. B. Wehrspohn, and U. Gösele, *J. Vac. Sci. Technol. B* **21**, 763 (2003).

<sup>11</sup>A. P. Li, F. Müller, and U. Gösele, *Electrochem. Solid-State Lett.* **3**, 131 (2000).

<sup>12</sup>C. Y. Liu, A. Datta, and Y. L. Wang, *Appl. Phys. Lett.* **78**, 120 (2001).

<sup>13</sup>C. Y. Liu, A. Datta, N. W. Liu, C. Y. Peng, and Y. L. Wang, *Appl. Phys. Lett.* **84**, 2509 (2004).

<sup>14</sup>Z. Sun and H. K. Kim, *Appl. Phys. Lett.* **81**, 3458 (2002).

<sup>15</sup>N. W. Liu, A. Datta, C. Y. Liu, and Y. L. Wang, *Appl. Phys. Lett.* **82**, 1281 (2003).

<sup>16</sup>A. P. Li, F. Müller, A. Birner, K. Nielsch, and U. Gösele, *J. Appl. Phys.* **84**, 6023 (1998).

<sup>17</sup>T. Xu, G. Zangari, and R. M. Metzger, *Nano Lett.* **2**, 37 (2002).

<sup>18</sup>H. Asoh and K. Nishio, *J. Vac. Sci. Technol. B* **19**, 569 (2001).

<sup>19</sup>D. Crouse and Y.-H. Lo, *Appl. Phys. Lett.* **76**, 49 (2000).

<sup>20</sup>Y. Kanamori and K. Hane, *Appl. Phys. Lett.* **78**, 142 (2001).